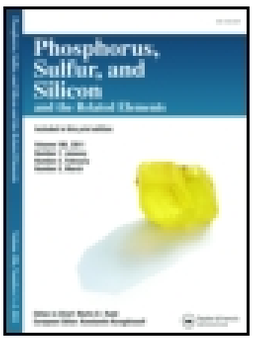

Taylor & Francis
Taylor & Francis Group

Phosphorus, Sulfur, and Silicon and the Related Elements

ISSN: 1042-6507 (Print) 1563-5325 (Online) Journal homepage: http://www.tandfonline.com/loi/gpss20

Phenol-formaldehyde resin route to the synthesis of several iron group transition metal phosphides

Hanchuan Zhao, Yan Shi, Zhiwei Yao, Liying Liang, Siqi Wang, Qingyou Liu, Baojiang Jiang & Yue Sun

To cite this article: Hanchuan Zhao, Yan Shi, Zhiwei Yao, Liying Liang, Siqi Wang, Qingyou Liu, Baojiang Jiang & Yue Sun (2018): Phenol-formaldehyde resin route to the synthesis of several iron group transition metal phosphides, Phosphorus, Sulfur, and Silicon and the Related Elements, DOI: 10.1080/10426507.2018.1550644

To link to this article: https://doi.org/10.1080/10426507.2018.1550644

Published online: 30 Dec 2018.

PHOSPHORUS, SULFUR, AND SILICON AND THE RELATED ELEMENTS
https://doi.org/10.1080/10426507.2018.1550644

Phenol-formaldehyde resin route to the synthesis of several iron group transition metal phosphides

Hanchuan Zhao[a], Yan Shi[a], Zhiwei Yao[a], Liying Liang[a], Siqi Wang[a], Qingyou Liu[b], Baojiang Jiang[c], and Yue Sun[a]

[a]Department of Petrochemical Engineering, College of Chemistry, Chemical Engineering and Environmental Engineering, Liaoning Shihua University, Fushun, P.R. China; [b]Key Laboratory of High-temperature and High-pressure Study of the Earth's Interior, Institute of Geochemistry, Chinese Academy of Sciences, Guiyang, P.R. China; [c]Key Laboratory of Functional Inorganic Material Chemistry, Ministry of Education of the People's Republic of China, Heilongjiang University, Harbin, P.R. China

ABSTRACT

A series of iron, cobalt and nickel metal phosphides of chemical formula Fe_xP, Co_2P and Ni_2P with high specific surface areas of 331.1, 294.2 and 228.0 $m^2\ g^{-1}$, respectively, was firstly synthesized by phenol-formaldehyde resin route. It was found that the as-prepared Co_2P and Ni_2P samples synthesized using phenol-formaldehyde resin as a carbon source showed much higher BET surface areas than those prepared using other carbon sources reported before, including cinnamic strong alkali anion exchange resin, *p*-phenylenediamine and hexamethylenetetramine. This phenol-formaldehyde resin route was proved to be as universal as traditional H_2 reduction method.

ARTICLE HISTORY
Received 21 September 2018
Accepted 17 November 2018

KEYWORDS
Fe_xP; Co_2P; Ni_2P; phenol-formaldehyde resin; transition metal phosphide

GRAPHICAL ABSTRACT

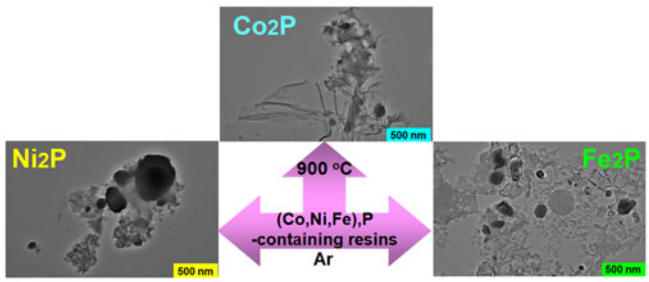

Introduction

Transition metal phosphides have attracted considerable attention for recent years because these materials are widely used in various fields, including photonics, magnetism, electronics, catalysis and so on.[1–4] In particular, metal phosphides have shown high catalytic activities for several reactions such as hydrogenation and hydrotreating,[5,6] N_2H_4 decomposition,[7–9] NO reduction[10,11] hydrogen evolution reaction,[12–15] and dry reforming of methane.[16] With the development of metal phosphide materials in various application fields, more and more efforts have been focused on synthetic methods for preparing metal phosphides. During the last twenty years, the major methods for the preparation of metal phosphides have been summarized by Carenco et al.[17] Among these routes, several synthetic methods, namely the reduction of metal phosphate in H_2 or H_2 plasma,[18–20] the phosphidation of metal or metal oxide with PH_3/H_2[21] and the thermal decomposition of metal oxide and hypophosphite precursor,[22] were usually used for the synthesis of transition metal phosphides for use as catalysts. With the increase of carbon materials as promising supports in many metal phosphide-related catalyst systems,[23–26] another strategy was to develop a carbothermal reduction method using various carbon sources (such as active carbon,[27] carbon nanotubes (CNTs),[28] *p*-phenylenediamine,[29] hexamethylenetetramine (HMT)[30] and resorcinol/formaldehyde[31]) for the synthesis of carbon supported phosphide catalysts.

Recently we developed a novel resin (e.g. cinnamic strong alkali anion exchange resin and phenolformaldehyde resin (PFR)) based carbon source for the synthesis of carbon supported phosphides.[32,33] Only two types of carbon supported phosphides (MoP/C and Ni_2P/C) can be prepared using the resin carbon sources. In this study, we further expand the

CONTACT Qingyou Liu liuqingyou@vip.gyig.ac.cn Key Laboratory of High-temperature and High-pressure Study of the Earth's Interior, Institute of Geochemistry, Chinese Academy of Sciences, Guiyang, 550081, P.R. China.
Color versions of one or more of the figures in the article can be found online at www.tandfonline.com/gpss.

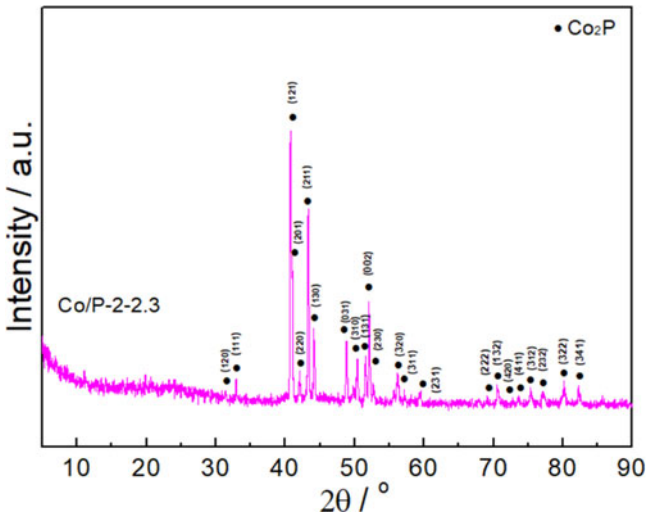

Figure 1. XRD patterns of the Co,P-containing resin precursor with a Co:P molar ratio of 2 and a PFR:Co mass ratio of 2.3 treated at 900 °C under an Ar atmosphere.

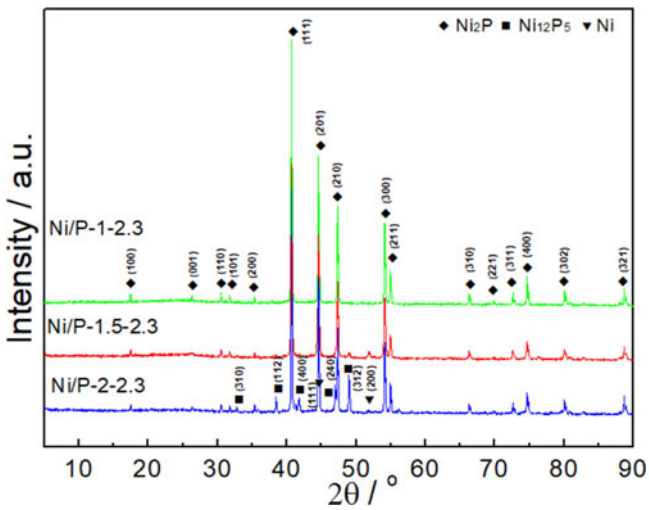

Figure 2. XRD patterns of the Ni,P-containing resin precursors with a Ni:P molar ratio of 2, 1.5 or 1 and a PFR:Co mass ratio of 2.3 treated at 900 °C under an Ar atmosphere.

application of phenolformaldehyde resin as a carbon source for the preparation of several iron group transition metal (Fe, Co and Ni) phosphides supported on carbon. This phenolformaldehyde resin route was found to be as universal as H_2 reduction method[18–20] (the most common method for the preparation of various phosphide catalysts).

Results and discussion

Microstructural characterization

Figures 1–3 shows the XRD patterns of the various M,P-containing resin precursors (M:P molar ratio= 2, 1.5 or 1 and PFR:M mass ratio =3.5 or 2.3 (M = Fe, Co and Ni)) treated at 900 °C under an Ar atmosphere. It can be seen from Figure 1 that the as-obtained product (Co/P-2-2.3) showed the main diffraction peaks at 40.7, 41.0, 43.3, 44.1, 48.7, 50.4, 51.5 and 52.0°, corresponding to the (121), (201), (211), (130), (031), (310), (131) and (002) reflections of

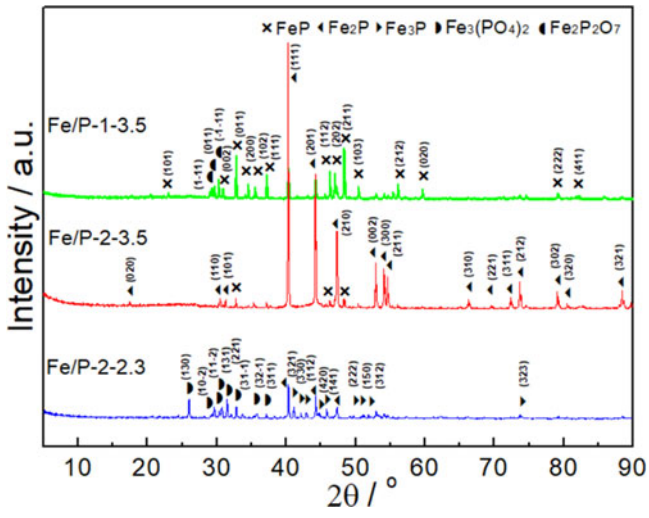

Figure 3. XRD patterns of the Fe,P-containing resin precursors with a Fe:P molar ratio of 2 or 1 and a PFR:Fe mass ratio of 2.3 or 3.5 treated at 900 °C under an Ar atmosphere.

Co_2P (PDF-00-032-0306), respectively. There were no peaks that can be assigned to Co oxides, Co phosphates or other Co phosphides, indicating that the pure Co_2P can be obtained using the current synthesis conditions.

In the case of the Ni,P-containing resin precursors (Figure 2), when the Ni:P molar ratio was 2 and the PFR:Ni mass ratio was 2.3, the as-obtained product (Ni/P-2-2.3) demonstrated the diffraction peaks of Ni_2P (major, $2\theta = 40.7$, 44.7, 47.4, 54.2, 55.0 and 74.8°, corresponding respectively to (111), (201), (210), (300), (211) and (400) planes, PDF-01-074-1385), $Ni_{12}P_5$ ($2\theta = 38.4$, 41.7, 47.0 and 49.0°, corresponding respectively to (112), (400), (240) and (312) planes, PDF-01-074-1381) and Ni (very minor, $2\theta = 44.3$ and 51.7°, corresponding respectively to (111) and (200) planes, PDF-01-070-1849). In view of the fact that the loss of phosphorus was unavoidable in the preparation process of Ni phosphide,[34,35] the excess phosphorus might be necessary in the preparation of phase-pure Ni_2P.[34] In order to obtain phase-pure Ni_2P, the Ni:P molar ratio was decreased to 1.5 and 1. When the Ni:P molar ratio was decreased to 1.5, a very small amount of $Ni_{12}P_5$ and Ni phases were also observed. With a further decrease in the Ni:P molar ratio, the $Ni_{12}P_5$ and Ni phases completely disappeared, and the pure Ni_2P phase can be obtained at a Ni:P molar ratio of 1.

As for the Fe,P-containing resin precursors (Figure 3), when the Fe:P molar ratio was 2 and PFR:Fe mass ratio was 2.3, the as-obtained product (Fe/P-2-2.3) was a mixture of Fe_2P (main diffraction peaks at $2\theta = 40.3$, 44.2, 47.3, 53.0, 54.1 and 54.6°, due respectively to (111), (201), (210), (002), (300) and (211) planes, PDF-01-088-1803), Fe_3P (main diffraction peaks at $2\theta = 41.0$, 42.1, 2.3, 44.5, 45.8, 49.7, 51.1 and 51.8°, assigning respectively to (321), (330), (112), (420), (141), (222), (150) and (312) planes, PDF-01-089-2712) and $Fe_3(PO_4)_2$ (main diffraction peaks at $2\theta = 26.0$, 29.6, 30.6, 30.7, 31.4 and 32.8°, corresponding respectively to (130), (10-2), (11-2), (131), (221) and (31-1) planes, PDF-00-035-0357). The result indicated that the amount of PRF might be not enough for the reduction reaction due to the

Table 1. Metal phosphide phases obtained from the precursors with different M:P molar ratios and PFR:M mass ratios (M = Fe, Co, Ni).

Sample	Metal phosphide phases	JCPDS cards
CoP-2-2.3	Co_2P	00-032-0306
NiP-2-2.3	Ni_2P, $Ni_{12}P_5$, Ni	01-074-1385, 01-074-1381, 01-070-1849
NiP-1.5-2.3	Ni_2P, $Ni_{12}P_5$, Ni	01-074-1385, 01-074-1381, 01-070-1849
NiP-1-2.3	Ni_2P	01-074-1385
FeP-2-2.3	Fe_2P, Fe_3P, $Fe_3(PO_4)_2$	01-088-1803, 01-089-2712, 00-035-0357
FeP-2-3.5	Fe_2P, FeP (very minor)	01-088-1803, 01-078-1443
FeP-1-3.5	Fe_2P, FeP, $Fe_2P_2O_7$	01-088-1803, 01-078-1443,01-072-1516

formation of $Fe_3(PO_4)_2$. When the PFR:Fe mass ratio was increased to 3.5, the product was almost Fe_2P with a very small amount of FeP impurity. In order to try to obtain single-phase FeP, the PFR:Fe mass ratio remained unchanged and the Fe:P molar ratio was adjusted to 1:1. Unfortunately, the resultant sample was just the mixed phases of Fe_2P, FeP, $Fe_2P_2O_7$.

For the sake of comparison, Table 1 lists the various metal phosphide phases obtained in the study. It was clear that pure Co_2P can be obtained from its corresponding precursor with a stoichiometric ratio of 2:1 Co:P and a lower PFR:M (M = Co) mass ratio of 2.3. However, the preparation of Ni_2P and Fe_xP was not as easy as that of Co_2P because it depended on the initial M/P molar ratio or the PFR:M mass ratio (M = Ni or Fe). Fortunately, the pure Ni_2P can be obtained by decreasing Ni:P molar ratio from 2 to 1, and the Fe_xP product can be obtained by increasing PFR:Fe mass ratio from 2.3 to 3.5.

The BET surface areas of as-prepared Co_2P, Ni_2P and Fe_xP samples using PFR as a carbon source were measured by surface area analyzer, and they were compared with those of corresponding phosphides prepared using other carbon sources in previous studies. It can be observed from Table 2 that the specific surface areas of Co_2P, Ni_2P and Fe_xP obtained in this work were 331.1, 294.2 and 228.0 $m^2 \cdot g^{-1}$, respectively. Since the specific surface area of the carbonized PFR resin was reported to be very low (2.5 $m^2 \cdot g^{-1}$),[33] these high specific surface areas should be attributed to the formation of metal phosphides. It was worthy to note that the Co_2P and Ni_2P synthesized using PFR showed much higher BET surface areas than those prepared using other carbon sources (e.g. D201, *p*PDA and HMT).

Subsequently, the morphologies of as-prepared Co_2P, Ni_2P and Fe_xP samples using PFR as a carbon source were characterized by SEM and TEM. Figure 4 shows the SEM images of Co_2P, Ni_2P and Fe_xP obtained in this study and the corresponding EDX analysis results are listed in Table 3. It can be observed from Figure 4 that the morphologies of Co_2P, Ni_2P and Fe_xP were very similar and they were composed of dispersed near-spherical nanoparticles with the size range below ~500 nm. Noticeably, it was clear that these divided nanoparticles connected with each other through thin sheets. These sheets might be carbon deposites from resin decomposition because a large amount of carbon was detected by EDX (Table 3). And the EDX gave the product composition including M, P, C and O elements (M = Co, Ni and Fe). It was also indicated that the M/P molar ratios were 2.06, 2.02 and 2.05 for Co_2P, Ni_2P and Fe_xP, respectively, which were a little higher than the expected

Table 2. BET surface areas of metal phosphides synthesized using different solid-state carbon sources.

Carbon source	Metal phosphide	S_{BET} ($m^2 \cdot g^{-1}$)	Ref.
PFR	Co_2P	331.1	This work
PFR	Ni_2P	294.2	This work
PFR	Fe_xP	228.0	This work
D201	Ni_2P	69.3	[32]
*p*PDA	Ni_2P	203.2	[29]
HMT	Ni_2P	191.7	[30]
HMT	Co_2P	43.6	[30]

PFR = phenol-formaldehyde resin; D201 = cinnamic strong alkali anion exchange resin; *p*PDA = *p*-phenylenediamine; HMT = hexamethylenetetramine.

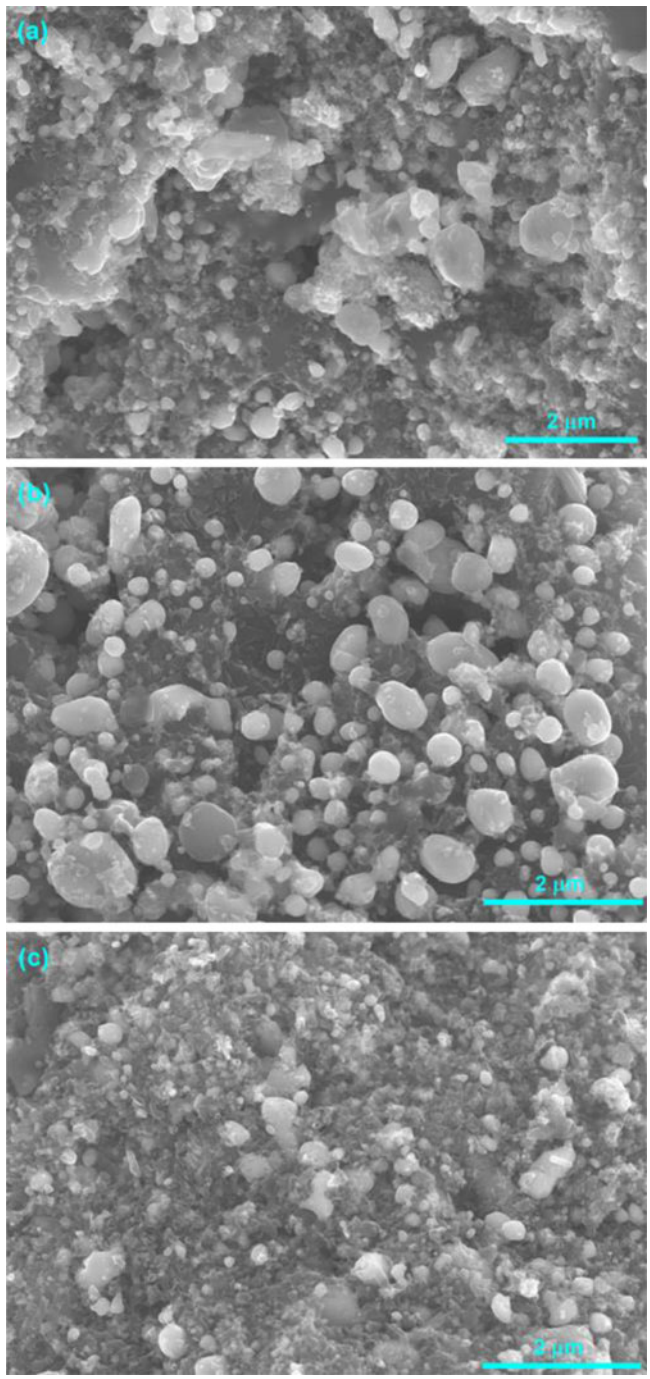

Figure 4. SEM images of (a) Co_2P, (b) Ni_2P and (c) Fe_xP products.

stoichiometric value for Co_2P, Ni_2P and Fe_2P. Wang et al reported that, although the preparations were carried out with stoichiometric quantities of phosphorus and metal and

Table 3. SEM/EDX surface elemental analysis results.

Sample	M[a] (at %)	P (at %)	O (at %)	C (at %)	M/P atomic ratio[a]
Co_2P	7.2	3.5	7.5	81.8	2.06
Ni_2P	9.9	4.9	8.9	76.3	2.02
Fe_xP	7.6	3.7	6.8	81.9	2.05

[a]M = Co, Ni, Fe.

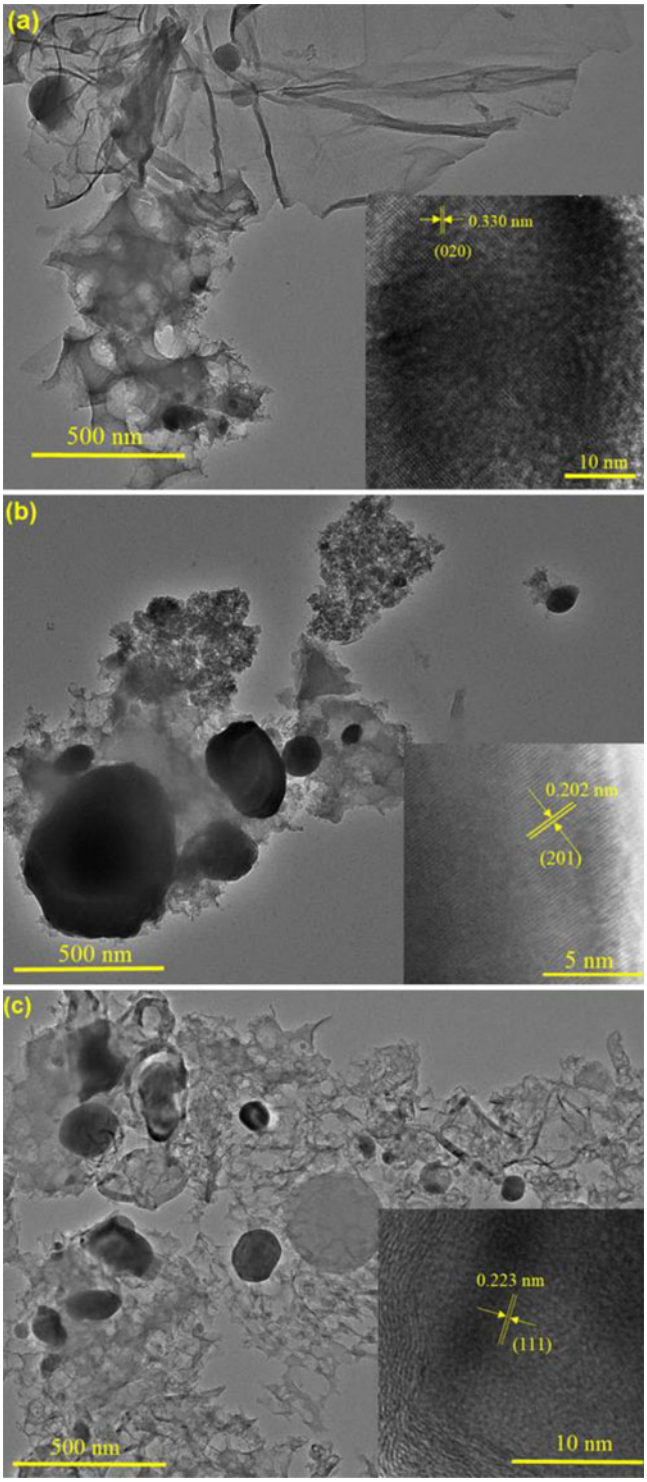

Figure 5. TEM images of (a) Co_2P, (b) Ni_2P and (c) Fe_xP products. The insets show the corresponding Co_2P (020), Ni_2P (201) and Fe_2P (111) crystal lattices.

even excess phosphorus, the final products tended to be metal-rich due to the loss of phosphorus in the preparation processes.[32] The SEM results were in good agreement with

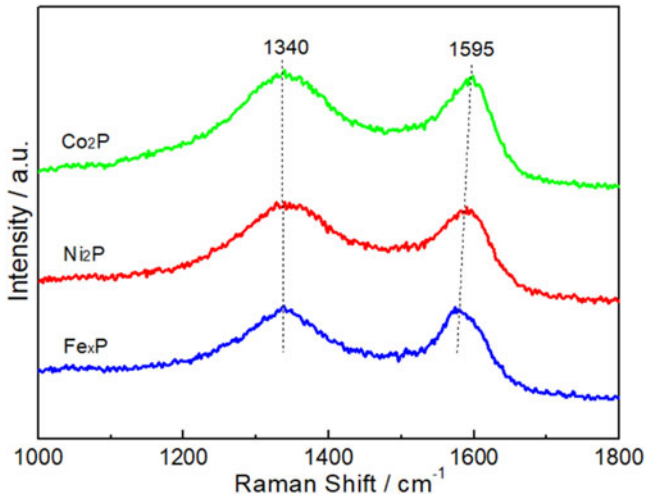

Figure 6. Raman spectra of the Co_2P, Ni_2P and Fe_xP products.

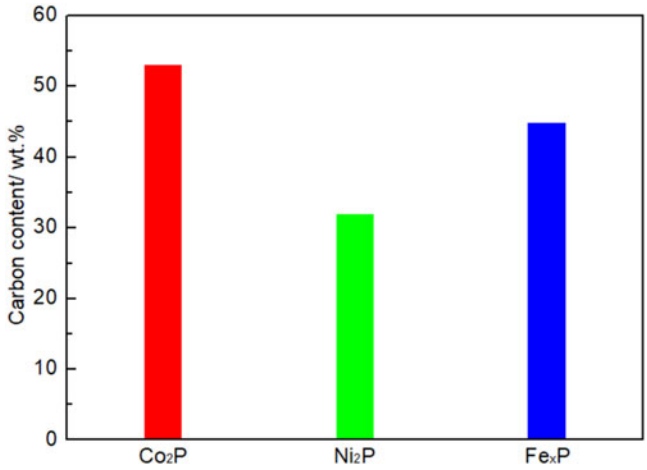

Figure 7. Carbon contents of the Co_2P, Ni_2P and Fe_xP products.

the observation of TEM images (Figure 5). It can be seen from Figure 5 that the particle size ranges of Co_2P, Ni_2P and Fe_xP were 25–150, 80–500 and 50–200, respectively. Although bigger particles were observed, especially for the Ni_2P sample, they were well dispersed on the carbon. This was probably the reason why the Co_2P, Ni_2P and Fe_xP samples showed high BET surface areas (see Table 2). Additionally, the insets clearly showed that the measured spacing between any two adjacent lattice fringes were 0.330, 0.202 and 0.223 nm, which were consistent with the d-spacings of the (020) plane of Co_2P, the (201) plane of Ni_2P and the (111) plane of Fe_2P, respectively.

Finally, the information regarding the carbon formation during carbonization process was obtained by Raman spectroscopy. It can be seen form Figure 6 that there were two intense bands attributed to the disorder band (D-band) and the tangential band (G-band) of carbon species. The G-band (at ~1595 cm^{-1}), which derived from the vibration of sp^2 hybridized carbon in the two-dimensional graphite for ordered carbon species, and the D-band was highly sensitive to amorphous carbon or defects in carbon materials and appeared at ~1340 cm^{-1}.[36–40] The carbon contents of the Co_2P, Ni_2P and Fe_xP products were determined by CHN-O-Rapid analyzer. It can be observed from Figure 7 that the

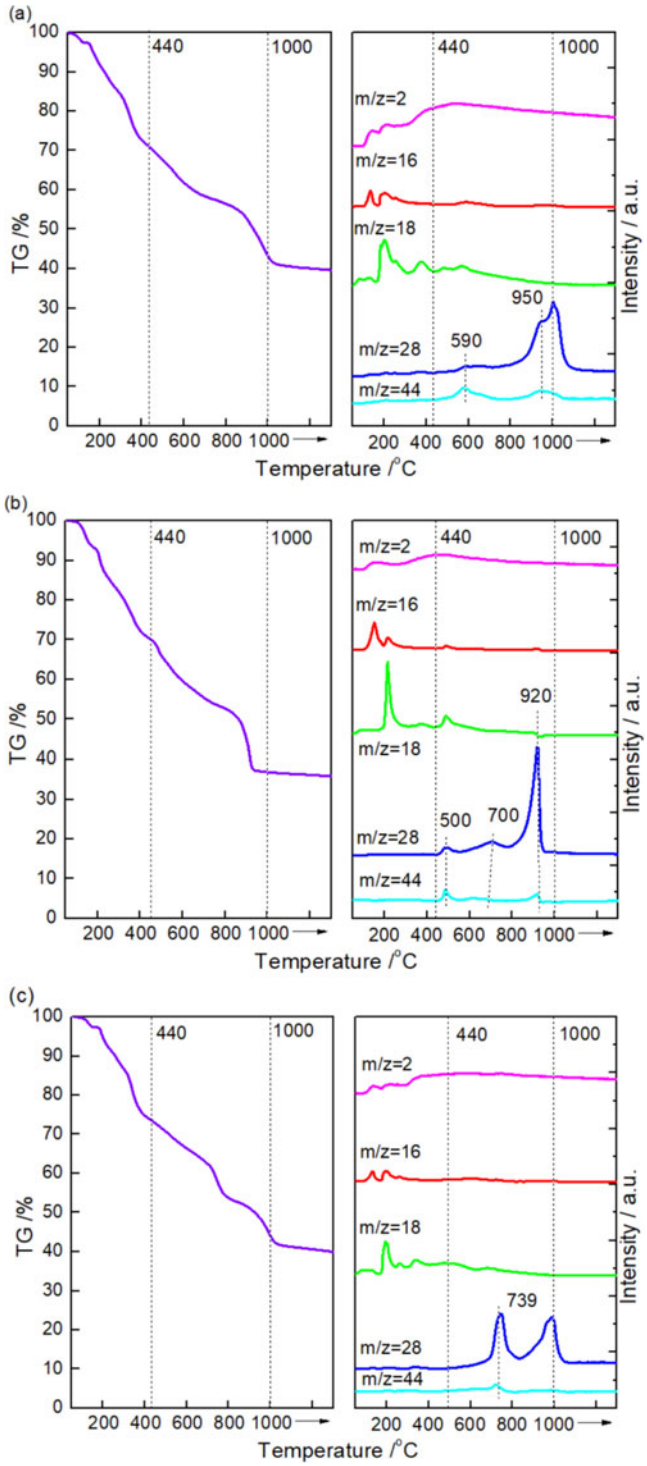

Figure 8. TG-MS profiles of the metal, P-containing resin precursors ((a) for Co_2P, (b) for Ni_2P and (c) for Fe_xP).

carbon contents of Co_2P, Ni_2P and Fe_xP obtained in this work were 53.1, 32.0 and 44.9 wt%, respectively.

Formation process

To investigate the formation process of Co_2P, Ni_2P and Fe_xP, the thermal treatment processes of the metal,P-containing resin precursors were followed by TG-MS. It was believed that the carbonization processes of metal,P-containing resin precursors usually involved two temperature regions: low temperature range and high temperature range.[32,33] In this study, the low temperature range and high temperature range were ≤440 °C and 440–1000 °C, respectively (see Figure 8). In the low temperature range, a successive sharp mass loss was observed on the TG profiles, which should be due to the dehydration reactions of resin besides the decomposition of metal and phosphonium salts,[32,33] because a large quantity of multi-component gases were detected by MS and the simultaneous signals of $m/z = 2$, 16 and 18 corresponded to H_2, CH_4 and H_2O, respectively. In the high temperature range, another sharp mass loss and a large amount of CO ($m/z = 28$) and CO_2 ($m/z = 44$) besides H_2, CH_4 and H_2O were observed on the TG-MS profiles. The results indicated that besides the deep carbonization of the resin, strong redox reactions occurred at higher temperatures, which led to a complete transformation of oxidized species into Co_2P, Ni_2P and Fe_xP (see Figures 1–3). Since no signal of PH_3 was detected in the MS signal, Co, Ni and Fe species should be phosphided by PO_x, as suggested before.[32,33]

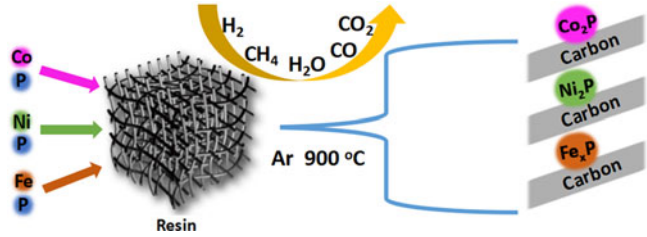

Figure 9. Scheme of the formation mechanism of metal phosphides in the resin-based route.

Based on the results of TG-MS, XRD, SEM, TEM and elemental analysis, the formation mechanism of metal phosphides in the resin-based route was described as follows (see Figure 9): the PFR with a network structure was firstly carbonized to produce C, H_2, CH_4 and H_2O, and then the M (M = Co, Ni and Fe),P-containing species mixed with the PFR were reduced by C above 900 °C, to produce metal phosphides located around carbon, with the release of CO and CO_2.

Experimental

Sample preparation

In this study, the phosphides of metals (Fe, Co and Ni) were prepared simply in two steps. Firstly, the precursors for phosphides were prepared by mechanical mixing method through co-grinding phenol-formaldehyde resin (PFR), metal oxide (Fe_2O_3, Co_3O_4 and NiO, obtained by calcination of $Fe(NO_3)_3{\cdot}9H_2O$, $Co(NO_3)_2{\cdot}6H_2O$, $Ni(NO_3)_2{\cdot}6H_2O$), respectively) and $(NH_4)_2HPO_4$ (M:P molar ratio= 2, 1.5 or 1 and PFR:M mass ratio = 3.5 or 2.3 (M = Fe, Co and Ni)). Secondly, the precursor (~0.2 g) was heated in a quartz reactor with an inner diameter of 10 mm from room temperature (RT) to 900 °C at a rate of 10 °C min^{-1} under an Ar flow (50 mL min^{-1}) and maintained at this temperature for 1 h, followed by cooling to RT under Ar, and then passivated in a 1%O_2/Ar flow for 2 h.

Sample characterizations

X-ray diffraction (XRD) measurements were carried out using Cu Kα source with a X'Pert Pro MPD diffractometer. CHN elemental analyses were carried out on a Heraeus CHN-O-Rapid analyzer and the results were within ±0.4% of the theoretical values. The morphologies of the samples were characterized by scanning electron microscopy (SEM, Hitachi S-4800) equipped with energy dispersive X-ray spectroscopy (EDX) and transmission electron microscopy (TEM, Philips Tecnal 10). BET surface areas of the products were measured by a surface area analyzer (NOVA4200). Raman spectroscopy was carried out using a Horrba/Jobin-Yvon LABRAM-HR spectrometer with the 632.8 nm line of a helium-neon laser as excitation source. Thermogravimetry-mass spectrometry (TG-MS) experiments were performed using thermoanalyzer STA 449 F5 Jupiter coupled with quadrupolar mass-spectrometer QMS 403 D Aeolos. The samples were heated in a stream of pure Ar gas at a rate of 10 °C min^{-1} from 50 to 1000 °C. The traces of masses (m/z) with the increase of temperature were recorded as follows: $m/z = 2$, $m/z = 16$, $m/z = 18$, $m/z = 28$, $m/z = 40$ and $m/z = 44$.

Conclusions

In summary, a simple synthesis of a series of iron, cobalt and nickel metal phosphides of chemical formula Fe_xP, Co_2P and Ni_2P with high specific surface areas of 331.1, 294.2 and 228.0 $m^2\ g^{-1}$, respectively, was reported. The current approach used a phenol-formaldehyde resin as a reductant instead of H_2 and employed an inert gas as a feed gas. This phenol-formaldehyde resin route was found to be as universal as traditional H_2 reduction method and it was worthwhile to investigate their catalytic performance in the future.

Funding

The work was supported by the National Natural Science Foundation of China (No. 21276253), the Liaoning Province Natural Science Foundation (No. 20180551272) and the Project of Liaoning Province Department of Education (No. L2017LZD003).

ORCID

Zhiwei Yao http://orcid.org/0000-0002-2535-9808
Qingyou Liu http://orcid.org/0000-0002-5630-7680

References

[1] Alexander, A.-M.; Hargreaves, J. S. J. Alternative Catalytic Materials: Carbides, Nitrides, Phosphides and Amorphous Boron Alloys. *Chem. Soc. Rev.* 2010, *39*, 4388–4401. DOI: 10.1039/b916787k.

[2] Liang, Z.; Huo, R.; Yin, S.; Zhang, F.; Xu, S. Eco-efficient Synthesis Route of Carbon-Encapsulated Transition Metal Phosphide with Improved Cycle Stability for Lithium-Ion Batteries. *J. Mater. Chem. A.* 2014, *2*, 921–925. DOI: 10.1039/C3TA13879H.

[3] Yoon, K. Y.; Jang, Y.; Park, J.; Hwang, Y.; Koo, B.; Park, J.-G.; Hyeon, T. Synthesis of Uniform-Sized Bimetallic Iron-Nickel Phosphide Nanorods. *J. Solid State Chem.* 2008, *181*, 1609–1613. DOI: 10.1016/j.jssc.2008.05.022.

[4] Jiang, X.; Xiong, Q.; Nam, S.; Qian, F.; Li, Y.; Lieber, C. M. InAs/InP Radial Nanowire Heterostructures as High Electron Mobility Devices. *Nano Lett.* 2007, *7*, 3214–3218. DOI: 10.1021/nl072024a.

[5] Abu, I. I.; Smith, K. J. The Effect of Cobalt Addition to Bulk MoP and Ni_2P Catalysts for the Hydrodesulfurization of 4,6-dimethyldibenzothiphene. *J. Catal.* 2006, *241*, 356–366. DOI: 10.1016/j.jcat.2006.05.010.

[6] Wang, X.; Clark, P.; Oyama, S. T. Synthesis, Characterization, and Hydrotreating Activity of Several Iron Group Transition Metal Phosphides. *J. Catal.* 2002, *208*, 321–331. DOI: 10.1006/jcat.2002.3604.

[7] Ding, L.; Shu, Y.; Wang, A.; Zheng, M.; Li, L.; Wang, X.; Zhang, T. Preparation and Catalytic Performances of Ternary Phosphides NiCoP for Hydrazine Decomposition. *Appl. Catal. A.* 2010, *385*, 232–237. DOI: 10.1016/j.apcata.2010.07.020.

[8] Cheng, R.; Shu, Y.; Zheng, M.; Li, L.; Sun, J.; Wang, X.; Zhang, T. Molybdenum Phosphide, A New Hydrazine Decomposition Catalyst: Microcalorimetry and FTIR Studies. *J. Catal.* 2007, *249*, 397–400. DOI: 10.1016/j.jcat.2007.04.007.

[9] Zheng, M.; Shu, Y.; Sun, J.; Zhang, T. Carbon-Covered Alumina: A Superior Support of Noble Metal-Like Catalysts for Hydrazine Decomposition. *Catal. Lett.* 2008, *121*, 90–96. DOI: 10.1007/s10562-007-9300-9.

[10] Yao, Z.; Dong, H.; Shang, Y. Catalytic Activities of Iron Phosphide for NO Dissociation and Reduction with Hydrogen. *J. Alloys Compd.* 2009, *474*, L10–L13. DOI: 10.1016/j.jallcom.2008.06.072.

[11] Yao, Z.; Qiao, X.; Liu, D.; Shi, Y.; Zhao, Y. Catalytic Activities of Transition Metal Phosphides for NO Dissociation and Reduction with CO. *Chem. Biochem. Eng. Q.* 2016, *29*, 505–510. DOI: 10.15255/CABEQ.2014.2133.

[12] Feng, L.; Vrubel, H.; Bensimon, M.; Hu, X. Easily-Prepared Dinickel Phosphide (Ni_2P) Nanoparticles as an Efficient and Robust Electrocatalyst for Hydrogen Evolution. *Phys. Chem. Chem. Phys.* 2014, *16*, 5917–5921. DOI: 10.1039/c4cp00482e.

[13] Popczun, E. J.; McKone, J. R.; Read, C. G.; Biacchi, A. J.; Wiltrout, A. M.; Lewis, N. S.; Schaak, R. E. Nanostructured Nickel Phosphide as an Electrocatalyst for the Hydrogen Evolution Reaction. *J. Am. Chem. Soc.* 2013, *135*, 9267–9270. DOI: 10.1021/ja403440e.

[14] Popczun, E. J.; Read, C. G.; Roske, C. W.; Lewis, N. S.; Schaak, R. E. Highly Active Electrocatalysis of the Hydrogen Evolution Reaction by Cobalt Phosphide Nanoparticles. *Angew. Chem.* 2014, *126*, 5531–5534. DOI: 10.1002/ange.201402646.

[15] Li, T.; Jin, H.; Liang, Z.; Huang, L.; Lu, Y.; Yu, H.; Hu, Z.; Wu, J.; Xia, B.; Feng, G.; et al. Synthesis of Single Crystalline Two-Dimensional Transition-Metal Phosphides via a Salt-Templating Method. *Nanoscale* 2018, *10*, 6844–6849. DOI: 10.1039/C8NR01556B.

[16] Yao, Z.; Luan, F.; Sun, Y.; Jiang, B.; Song, J.; Wang, H. Molybdenum Phosphide as a Novel and Stable Catalyst for Dry Reforming of Methane. *Catal. Sci. Technol.* 2016, *6*, 7996–8004. DOI: 10.1039/C6CY00836D.

[17] Carenco, S.; Portehault, D.; Boissiere, C.; Mezailles, N.; Sanchez, C. Nanoscaled Metal Borides and Phosphides: Recent Developments and Perspectives. *Chem. Rev.* 2013, *113*, 7981–8065. DOI: 10.1021/cr400020d.

[18] Oyama, S. T. Novel Catalysts for Advanced Hydroprocessing: Transition Metal Phosphides. *J. Catal.* 2003, *216*, 343–352. DOI: 10.1016/S0021-9517(02)00069-6.

[19] Guan, J.; Wang, Y.; Qin, M.; Yang, Y.; Li, X.; Wang, A. Synthesis of Transition-Metal Phosphides from Oxidic

Precursors by Reduction in Hydrogen Plasma. *J. Solid State Chem*. 2009, *182*, 1550–1555. DOI: 10.1016/j.jssc.2009.03.026.

[20] Wang, A.; Qin, M.; Guan, J.; Wang, L.; Guo, H.; Li, X.; Wang, Y.; Prins, R.; Hu, Y. Synthesis of Metal Phosphides: Reduction of Oxide Precursors in a Hydrogen Plasma. *Angew. Chem*. 2008, *120*, 6141–6143. DOI: 10.1002/ange.200801559.

[21] Yang, S.; Liang, C.; Prins, R. A Novel Approach to Synthesizing Highly Active Ni_2P/SiO_2 Hydrotreating Catalysts. *J. Catal*. 2006, *237*, 118–130. DOI: 10.1016/j.jcat.2005.10.021.

[22] Guan, Q.; Li, W. A Novel Synthetic Approach to Synthesizing Bulk and Supported Metal Phosphides. *J. Catal*. 2010, *271*, 413–415. DOI: 10.1016/j.jcat.2010.02.031.

[23] Lu, Y.; Tu, J.; Xiong, Q.; Xiang, J.; Mai, Y.; Zhang, J.; Qiao, Y.; Wang, X.; Gu, C.; Mao, S. X. Controllable Synthesis of a Monophase Nickel Phosphide/Carbon (Ni_5P_4/C) Composite Electrode via Wet-Chemistry and a Solid-State Reaction for the Anode in Lithium Secondary Batteries. *Adv. Funct. Mater*. 2012, *22*, 3927–3935. DOI: 10.1002/adfm.201102660.

[24] Yan, Y.; Zhao, B.; Yi, S. C.; Wang, X. Assembling Pore-Rich FeP Nanorods on the CNT Backbone as an Advanced Electrocatalyst for Oxygen Evolution. *J. Mater. Chem. A*. 2016, *4*, 13005–13010. DOI: 10.1039/C6TA05317C.

[25] Chang, J.; Xiao, Y.; Xiao, M.; Ge, J.; Liu, C.; Xing, W. Surface Oxidized Cobalt-Phosphide Nanorods as an Advanced Oxygen Evolution Catalyst in Alkaline Solution. *ACS Catal*. 2015, *5*(11), 6874–6878. DOI: 10.1021/acscatal.5b02076.

[26] Wang, D.; Shen, Y.; Zhang, X.; Wu, Z. Enhanced Hydrogen Evolution from the MoP/C Hybrid by the Modification of Ketjen Black. *J. Mater. Science*. 2017, *52*(6), 3337–3343. DOI: 10.1007/s10853-016-0621-1.

[27] Yao, Z. Exploration on Synthesis of Activated Carbon Supported Molybdenum Carbide, Nitride and Phosphide via Carbothermal Reduction Route. *J. Alloys Compd*. 2009, *475*, L38–L41. DOI: 10.1016/j.jallcom.2008.07.130.

[28] Yao, Z.; Hai, H.; Lai, Z.; Zhang, X.; Peng, F.; Yan, C. A Novel Carbothermal Synthesis Route for Carbon Nanotube Supported Fe_2P Nanoparticles. *Top. Catal*. 2012, *55*, 1040–1045. DOI: 10.1007/s11244-012-9885-0.

[29] Liang, P.; Liang, F.; Yao, Z.; Gao, H.; Sun, Y.; Jiang, B.; Tong, J. Novel Synthesis of Dispersed Nickel Phosphide Nanospheres on Carbon Support via Carbothermal Reduction Route. *Phosphorus Sulfur Silicon Relat. Elem*. 2017, *192*, 812–818. DOI: 10.1080/10426507.2017.1286493.

[30] Yao, Z.; Wang, G.; Shi, Y.; Zhao, Y.; Jiang, J.; Zhang, Y.; Wang, H. One-Step Synthesis of Nickel and Cobalt Phosphide Nanomaterials via Decomposition of Hexamethylenetetramine-Containing Precursors. *Dalton Trans*. 2015, *44*, 14122–14129. DOI: 10.1039/C5DT02319J.

[31] Wang, H.; Shu, Y.; Wang, A.; Wang, J.; Zheng, M. One-Pot Synthesis and Characterization of Metal Phosphide-Doped Carbon Xerogels. *Carbon* 2008, *46*, 2076–2082. DOI: 10.1016/j.carbon.2008.08.021.

[32] Yao, Z.; Tong, J.; Qiao, X.; Jiang, J.; Zhao, Y.; Liu, D.; Zhang, Y.; Wang, H. Novel Synthesis of Dispersed Molybdenum and Nickel Phosphides from Thermal Carbonization of Metal-and Phosphorus-Containing Resins. *Dalton Trans*. 2015, *44*, 19383–19391. DOI: 10.1039/C5DT02464A.

[33] Song, T.; Shi, Y.; Yao, Z.; Gao, H.; Liang, F.; Jiang, B.; Sun, Y.; Kong, L. A Facile Route for Large-Scale Synthesis of Molybdenum Phosphide Nanoparticles with High Surface Area. *Phosphorus Sulfur Silicon Relat. Elem*. 2017, *192*, 1159–1164. DOI: 10.1080/10426507.2017.1330829.

[34] Liu, X.; Xu, L.; Zhang, B. Essential Elucidation for Preparation of Supported Nickel Phosphide Upon Nickel Phosphate Precursor. *J. Solid State Chem*. 2014, *212*, 13–22. DOI: 10.1016/j.jssc.2014.01.009.

[35] Sawhill, S. J.; Layman, K. A.; Van Wyk, D. R.; Engelhard, M.H.; Wang, C.; Bussell, M. E. Thiophene Hydrodesulfurization Over Nickel Phosphide Catalysts: Effect of the Precursor Composition and Support. *J. Catal*. 2005, *231*, 300–313. DOI: 10.1016/j.jcat.2005.01.020.

[36] Zhao, Y.; Yao, Z.; Shi, Y.; Qiao, X.; Wang, G.; Wang, H.; Yin, J.; Peng, F. A Novel Approach to the Synthesis of Bulk and Supported β-Mo_2C Using Dimethyl Ether as a Carbon Source. *New J. Chem*. 2015, *39*, 4901–4908. DOI: 10.1039/C5NJ00395D.

[37] Yao, Z.; Jiang, J.; Zhao, Y.; Luan, F.; Jiang, Z.; Shi, Y.; Gao, H.; Wang, H. Insights into the Deactivation Mechanism of Metal Carbide Catalysts for Dry Reforming of Methane via Comparison of Nickel-Modified Molybdenum and Tungsten Carbides. *RSC Adv*. 2016, *6*, 19944–19951. DOI: 10.1039/C5RA24815A.

[38] Gao, H.; Yao, Z.; Shi, Y.; Jia, R.; Liang, F.; Sun, Y.; Mao, W.; Wang, H. Simple and Large-Scale Synthesis of β-Phase Molybdenum Carbides as Highly Stable Catalysts for Dry Reforming of Methane. *Inorg. Chem. Front*. 2018, *5*, 90–99. DOI: 10.1039/C7QI00532F.

[39] Gao, H.; Yao, Z.; Shi, Y.; Wang, S. Improvement of the Catalytic Stability of Molybdenum Carbide via Encapsulation Within Carbon Nanotubes in Dry Methane Reforming. *Catal. Sci. Technol*. 2018, *8*, 697–701. DOI: 10.1039/C7CY02506H.

[40] Bettahalli, N. M.; Vicente, J.; Moroni, L.; Higuera, G. A.; van Blitterswijk, C. A.; Wessling, M.; Stamatialis, D. F. Integration of hollow fiber membranes improves nutrient supply in three-dimensional tissue constructs. *Catal. Sci. Technol*. 2017, *7*, 3312–3324. DOI: 10.1016/j.actbio.2011.06.012.